

Global Precipitation During the 1997-98 El Niño and Initiation of the 1998-99 La Niña

By

Scott Curtis

Joint Center for Earth Systems Technology
University of Maryland Baltimore County
Laboratory for Atmospheres
NASA/Goddard Flight Center

and

Robert Adler,

Laboratory for Atmospheres
NASA/Goddard Flight Center

George Huffman, Eric Nelkin, David Bolvin

Science Systems Applications Inc.
Laboratory for Atmospheres
NASA/Goddard Flight Center

Abstract:

The 1997-99 ENSO cycle was very powerful, but also well observed. The best satellite rainfall estimates combined with gauge observations allow for a global analysis of precipitation anomalies accompanying the 1997-98 El Niño and initiation of the 1998-99 La Niña. For the period April 1997 to March 1998 the central to eastern Pacific, southeastern and western U.S., Argentina, eastern Africa, South China, eastern Russia, and North Atlantic were all more than two standard deviations wetter than normal. During the same year the Maritime Continent, eastern Indian Ocean, subtropical North Pacific, northeastern South America, and much of the mid-latitude southern oceans were more than two standard deviations drier than normal. An analysis of the evolution of the El Niño and accompanying precipitation anomalies revealed that a dry Maritime Continent led the formation of the El Niño SST, while in the central Pacific, precipitation anomalies lagged the El Niño SST by a season. A rapid transition from El Niño to La Niña occurred in May 1998, but as early as October-November 1997 precipitation indices captured precursor changes in Pacific rainfall anomalies. Differences were found between observed and modeled (NCEP/NCAR reanalysis) precipitation anomalies for 1997 and 98. In particular, the model had a bias towards positive precipitation anomalies and the magnitudes of the anomalies in the equatorial Pacific were small compared to the observations. Also, the evolution of the precipitation field, including the drying of the Maritime Continent and eastward progression of rainfall in the equatorial Pacific, was less pronounced for the model compared to the observations. One degree daily estimates of rainfall show clearly the Madden-Julian Oscillation and related westerly wind burst events over the Maritime Continent, which are key indicators for the onset of El Niño.

1. Introduction

It can be argued that the 1997-98 El Niño was the strongest ENSO event ever recorded. The unusually warm waters of the equatorial Pacific were accompanied by changes in the large scale circulation, followed by precipitation anomalies ranging from severe drought to floods. The Maritime Continent, Amazon and Congo basins, and Central America experienced drought during some part of 1997 and 1998, while Argentina, Peru, and East Africa were hardest hit by flooding. In fact, there have been many studies documenting the variability of regional precipitation during the 97-98 event (Montroy et al. 1998, Bell and Halpert 1998, Bell et al. 1999, Jaksic 1998, Mullen 1998, Pavia and Badan 1998, Harrison and Larkin 1998, Kogan 1998, Jensen et al. 1998, McPhadden 1999). The El Niño was followed by a persistent La Niña. The regional precipitation anomalies for this phase of the ENSO cycle have been less well documented. In this study satellite observations and gauges are used to examine global precipitation anomalies associated with the 1997-98 El Niño and 1998-99 La Niña. Another focus is the timing of the onset and decay of precipitation anomalies over the Maritime Continent and East Pacific associated with the evolution of ENSO. Finally, the observations will be compared to model generated precipitation during this period.

An experimental version of the Global Precipitation Climatology Project's (GPCP) community data set (reference section 2) was used to construct precipitation anomalies for the year average April 1997 to March 1998 (Fig. 1). Overlain is Ropelewski and Halpert's (1987) (hereafter RH) schematic figure showing areas typically dry and wet during an El Niño. Ropelewski and Halpert's pioneering work was a compilation of regional studies of precipitation during ENSO. The paucity of surface

observations restricted a global analysis. Recent data products based on remotely sensed precipitation estimates invited a revisitation of global precipitation anomalies associated with ENSO events, in particular the powerful 97-98 event.

2. Data and Indices

The primary data source for this study is an experimental version of the Global Precipitation Climatology Project's (GPCP; Huffman et al. 1997) community data set, hereafter referred to as GPCPx. This data set is like Huffman et al. (1997) except there has been a slight modification in the merger technique; it uses TOVS data (Suskind et al. 1997) to fill in missing or uncertain data in the high latitudes, and the record extends from January 1979 to July 1999.

GPCPx is compared with NCEP/NCAR's reanalysis product (Kalnay et al. 1996). Precipitation is computed from a 62 wave triangular, 28 layer spectral model "Medium Range Forecast" run.

For the examination of smaller time and space scales, an experimental one degree daily (1DD; Huffman et al. 1999) precipitation analysis was used. 1DD includes precipitation estimates from geosynchronous IR, and TOVS. Each day of the daily combination is scaled such that each month of data sums to the corresponding GPCPx month of data. This is done to ensure consistency between GPCP products and introduce gauge data as a constraint on 1DD. The product currently extends from January 1997 to December 1998. NCEP/NCAR also produces a daily reanalysis precipitation data set, with zonal grid spacing of 1.875° , and this was used to compare with 1DD.

Finally, the ENSO was tracked using an observed SST anomaly data set at 0.5° resolution (Reynolds and Smith 1995).

Several indices were used to monitor monthly temperature and precipitation anomalies in the Pacific basin and Maritime Continent. Following the Climate Prediction Center's analysis, SST and precipitation were computed within the core of the Maritime Continent (INDO; Fig. 2). Nino 3.4 (Fig. 2) was chosen to quantify SST in the East Pacific. A precipitation index was also constructed for the Nino 3.4 block. In addition, area averages of precipitation, the size of INDO and Nino 3.4, were moved throughout larger domains encompassing the Maritime Continent (mc) and East Pacific (p) (Fig. 2) as described by Curtis and Adler (1999). Moving blocks are especially useful in describing precipitation because of the spatially varying nature of rainfall. The mc- value denotes the minimum value in the moving blocks found within mc and p+ the maximum value found within p. A_{mc-} and A_{p+} refer to the minimum and maximum precipitation anomalies respectively. Thus, these indices capture the centers of action over the Maritime Continent and central Pacific and can often lead fixed indices in detecting climate change. The normalized difference of A_{p+} minus A_{mc-} equals the El Niño Index (EI), a measure of the westward gradient of rainfall anomalies. The normalized difference of A_{mc+} minus A_{p-} equals the La Niña Index (LI), a measure of the eastward gradient of rainfall anomalies. The El Niño Index minus the La Niña Index yields the ENSO Precipitation Index (ESPI). The normalized ESPI has been shown to be well correlated with Nino 3.4 and Southern Oscillation Index (SOI) and a good measure of the strength of the Walker circulation (Curtis and Adler 1999).

3. Monthly SST and Precipitation for 1996-99

This section uses maps and indices of SST and precipitation to describe the evolution of the 1997-98 El Niño and initiation of the 1998-99 La Niña. In particular, the tropics are examined to identify SST and precipitation signals which may be precursors to the onset or decay of ENSO events.

3.1 Global Anomalies

Figs. 3 to 6 describe the evolution of the El Niño and initiation of the La Niña in terms of global GPCPx precipitation anomalies. Bimonthly averages remove the 30-60 day oscillations and are thus useful in analyzing interannual variability. The monthly GPCPx fields for 1997-99 and climatologies were also used in the analysis, but not shown here. 1995-96 was characterized by a mild La Niña. It was the fourth strongest according to 20 years of ESPI data, but relatively weak compared to long-term SST and SOI records. In January-February 1997 (Fig. 3a,b), the La Niña pattern was weak, with negative SST and precipitation anomalies in the central to east Pacific and wet conditions straddling the equator over the Maritime Continent. A dry anomaly extended from the eastern equatorial Indian Ocean to Indonesia. The relation between this feature and the onset of the El Niño will be described further in section 3.2.

In March-April 1997 a warm anomaly was located off the coast of Peru (Fig. 3c). In the East Pacific the typical double Intertropical Convergence Zone (ITCZ) was absent, while in the West Pacific the ITCZ and South Pacific Convergence Zone (SPCZ) were further apart than normal. This pattern of precipitation was consistent with negative precipitation anomalies over the Maritime Continent, extending eastward in a band along

the equator and positive rainfall anomalies located immediately to the north and south (Fig. 3d).

In May-June 1997 (Fig. 3e, f) warm El Niño waters had extended into the central Pacific and positive anomalies were found off the west coast of North America. The rain band accompanying the ITCZ had begun to broaden, intensify, and migrate southward, consistent with a weakening of the Walker circulation. Negative anomalies over Southeast Asia were produced by a delay in the onset of the 1997 summer monsoon.

In July-August 1997 (Fig. 3g, h) the positive precipitation anomalies in the equatorial Pacific continued to strengthen and the Asian monsoonal rainfall was heavier than normal.

By September-October 1997 (Fig. 4a, b) the Indian Ocean had begun to warm while rainfall increased over East Africa. At the same time there was a decrease in convective precipitation over the Congo and Amazon basins.

The temperature anomalies in the East Pacific reached a maximum in November-December 1997 (Fig. 4c). Precipitation within the SPCZ and Pacific ITCZ merged, forming a region of positive precipitation anomaly east of the date line (Fig. 4d). The Atlantic ITCZ was anomalously dry and northern Argentina and the Southeast U.S. were anomalously wet during these months.

The largest precipitation anomalies in the Pacific occurred during January-February 1998 (Fig. 4f) after the El Niño (in terms of SST) had begun to weaken (Fig. 4e). Anomalously dry regions straddled the wet equatorial Pacific, providing evidence that during this stage of the ENSO an anomalous meridional, rather than zonal, circulation was dominant (Curtis and Hastenrath 1997). This will be

discussed in the context of the transition from El Niño to La Niña in section 3.2. The North Pacific storm track crossed the west coast of North America further south than normal bringing dry conditions to coastal Alaska and heavy rains to the Pacific Northwest.

By March-April 1998 (Fig. 4g, h) positive precipitation anomalies in the eastern Pacific had weakened. Northeast Brazil was anomalously dry but the Maritime Continent drought had begun to end.

A weak El Niño (in terms of SST) in May-June 1998 was accompanied by mostly negative precipitation anomalies in the Pacific (Fig. 5a, b). However, rainfall anomalies in excess of 10 mm day^{-1} remained off the coast of Peru. Positive precipitation anomalies were replaced by negative anomalies in the Southeast U.S.

In July-August 1998 the SST pattern in the Pacific was more characteristic of a La Niña than an El Niño and the Walker circulation began to strengthen as positive precipitation anomalies covered the East Indian Ocean and western Maritime Continent and negative anomalies dominated the central equatorial Pacific (Fig. 5c, d).

September-October 1998 (Fig. 5e, f) was characterized by a strengthening La Niña and cooling of the Indian Ocean. Heavy rains accompanied the North American summer monsoon.

From November-December 1998 to March-April 1999 (Figs. 5g, h and 6) a steep gradient of anomalous precipitation was formed in the western Pacific, as the convection center of the Maritime Continent and SPCZ continued to intensify and the largest negative precipitation anomalies shifted westward. In early 1999 (Fig. 6) enhanced rainfall was observed over the Amazon basin and southeastern Africa, while the Indian

Ocean was covered by dry anomalies. In March-April 1999 (Fig 6c, d) the La Niña pattern remained strong in terms of SST and precipitation, but with positive precipitation anomalies located just south of the equator in the eastern Pacific. In fact, the La Niña has persisted through boreal summer 1999 (not shown here).

In summary, the dry anomalies over the Maritime Continent led the formation of the El Niño. However, the maximum precipitation anomalies over the central Pacific lagged the peak in the El Niño SSTs by a season. The largest precipitation anomalies were confined to the equatorial Pacific basin and Maritime Continent from April to September 1997; were found throughout the global tropics and subtropics at the end of 1997; and extended as far poleward as Alaska by the beginning of 1998. Whether or not these precipitation anomalies were forced solely by the El Niño remains unclear.

3.2 Indices

The monthly evolution of observed temperature and precipitation anomalies in the equatorial Pacific is captured by indices shown in Figs. 7-8. Bimonthly averages of precipitation remove the 30-60 day oscillation. Early indications of the 1997-98 El Niño can be found in the decrease in rainfall over the Maritime Continent as described by the downward turn in INDO precipitation (Fig. 7b) and Amc- (Fig. 7c) in September-October 1996. The indices actually crossed the zero line in November-December. In the next bi-month positive precipitation anomalies were found in the Pacific search area (Fig. 7c). The Nino 3.4 SST index bottomed out in December 1996 and climbed to positive values in March 1997. Thus, negative precipitation anomalies were found over the Maritime Continent (ref. Fig. 3b) before the increase in rainfall and warming of the equatorial

Pacific (ref. Fig. 3c,d). Interestingly, the positive precipitation and SST signals were not co-located at this time. The increase in rainfall occurred in the central Pacific, just off the equator, and the warm anomalies covered the equatorial cold tongue in the east Pacific (ref. Fig. 3c,d). In fact, the anomalously clear conditions and subsequent increase in solar radiation during this season may have served to strengthen the developing El Niño. By May-June positive SST anomalies had extended in to the central Pacific (Fig. 3e), providing the energy for convection in the Nino 3.4 region (Fig. 3f, Fig. 7b). The El Niño evolved with the SST leading the precipitation signal in the central Pacific by about a month. However, the decrease in convection over the Maritime Continent occurred well before a small decrease in the water temperature surrounding the islands (Fig. 7a,b). A direct relation between these two signals is not evident. Dry conditions over the Maritime Continent (Amc-) were most extreme in October-November 1997, nearly simultaneous with the peak in El Niño SSTs, but leading Ap+ (Fig. 7c).

During the maturation of the El Niño, in September-October 1997, the Amc+ and Ap- began to rise and fall respectively (Fig. 7d), giving the first indication of the coming La Niña. The negative precipitation anomalies in the Pacific were found to the north of the anomalous enhanced rainfall (Fig. 4b) and positive anomalies surfaced over New Guinea in November-December, spreading throughout the Maritime Continent by March-April 1998.

3.3 Synthesis

During the end of the 1995-96 La Niña dry anomalies were found over the eastern Maritime Continent. These anomalies merged with negative anomalies already established over the Pacific and, through increased short wave radiation, may have contributed to an intensification of the warming of the equatorial cold tongue. In turn, the warm waters favored enhanced convection. The Maritime Continent was driest and the central Pacific was warmest around October-November 1997. The maximum precipitation anomaly in the Pacific followed in January-February 1998. As the El Niño strengthened, early indications of the coming La Niña were observed in the central Pacific. A dipole pattern of wet anomalies along the equator and dry anomalies to the North was consistent with an intensified meridional-vertical circulation (Curtis and Hastenrath 1997) from July-August 1997 to May-June 1998. The negative precipitation anomalies in the Pacific preceded the positive anomalies over the Maritime Continent. In the second half of 1998 the positive anomalies dissipated in the Pacific and the negative anomalies intensified and shifted westward.

The precipitation anomalies accompanying the 97-98 El Niño are illustrated by the April 1997 to March 1998 average and standard deviations from the long-term mean (Fig. 1). RH's schematic areas are generally consistent with the GPCPx anomalies. However, for the 97-98 event the precipitation anomalies were larger at the west coast of the U.S. rather than further inland. In Africa the RH areas capture the fringes of the largest precipitation anomalies. The interior of India, northeast Australia, and the Pacific near 165° E and 10° N were mostly wet rather than dry. GPCPx also shows substantial rainfall anomalies over the oceans. During this time it was anomalously wet from the

coast of China eastward and dry to the North. RH captures the anomalous rains of the central Pacific but not the statistically significant anomalies of the East Pacific. Some northern high latitude regions, including Eurasia, Siberia, and Canada, and even Antarctica received precipitation amounts in excess of 2 standard deviations from the mean. However, the gauge quality is questionable over these land areas. The Drake Passage and other spots of the southern high latitude oceans were significantly dry.

Finally, $Ap+$ and $Amc-$ are combined to determine the largest westward gradient of anomalous precipitation. The resulting El Niño Index (EI) (ref. Section 2) is positive when the central to eastern Pacific is anomalously wet and Maritime Continent dry. The combination of $Ap-$ and $Amc+$ yields the strongest eastward gradient of anomalous precipitation denoted by the La Nina Index (LI) (ref. Section 2). The difference between the indices, or ENSO precipitation Index (ESPI), determines the dominant signal. These indices are plotted in Fig. 8. The EI and ESPI both peaked in September-October 1997 (Fig. 8), slightly leading Nino 3.4 SST (Fig. 7a) and somewhat before the occurrence of the largest precipitation anomalies in the Pacific (Fig. 7c). According to the ESPI and EI the 1997-98 El Niño event was the largest over the past 20 years (Curtis and Adler 1999).

4. Observed Versus Modeled Precipitation

The evolution of NCEP/NCAR derived precipitation shows some striking differences from the observations. The absolute magnitudes of the modeled NINO 3.4 and INDO precipitation indices are smaller than observed (Fig. 9a). For GPCPx, the INDO index reached a minimum well before NINO 3.4 reached a maximum. However, the model shows a simultaneous peak in the indices (Fig. 9a). The extremes of $Ap+$ and

Amc- associated with the El Niño occurred earlier for the reanalysis than for the observations (Fig. 9b). Finally, the timeseries plots of Amc+ and Ap- are different for GPCPx as compared to NCEP/NCAR, especially in 1997 when the observations give negative values for Amc+, whereas the modeled precipitation produces a local maximum (Fig. 9c).

Fig. 10 shows the April 1997 to March 1998 average for GPCPx, NCEP/NCAR, and the GPCPx minus NCEP/NCAR difference. Although the ENSO signal is present in the modeled precipitation anomalies, there are substantial differences in magnitude between the reanalysis and observed estimates. As noted in a recent study by Janowiak et al. (1998) comparing GPCP and NCEP/NCAR, the magnitudes of the reanalysis values are smaller than those observed on the interannual time scale. In the central Pacific only a small area of modeled precipitation anomalies is greater than 4 mm day^{-1} and none of the anomalies in the Maritime Continent are less than -4 mm day^{-1} (Fig. 10b). In fact, the maximum anomalous precipitation rate within the wet equatorial East Pacific is 7.7 mm day^{-1} for the observations as compared to 5.4 mm day^{-1} for the model, while the minimum anomalous precipitation rate over the Maritime Continent is -6.1 and -4.0 mm day^{-1} respectively. The NCEP/NCAR average map shows very wet anomalies over India and very dry anomalies over equatorial South America which were not observed (Fig. 10). Also, NCEP/NCAR anomalies tend to be predominantly positive (Janowiak et al. 1998).

5. Daily Precipitation for 1997-1998

Fig. 11 shows a global time-longitude diagram of daily precipitation averaged from 5° N to 5° S. The period is January 1 1997 to December 31 1998. The plot shows a Madden-Julian type oscillation, as three precipitating systems traveled from the Indian Ocean to the central Pacific before the January-February-March 1998 peak ENSO signal. The heaviest precipitation was located in the central Pacific in the second half of 1997, moving to the East Pacific by boreal spring 1998. Precipitation over the Maritime Continent was especially weak from July to October 1997, when the Walker circulation was weakest and ESPI was a maximum (Fig. 8), and strong in the second half of 1998. In May 1998 a precipitation complex, possibly associated with a Kelvin wave, traveled from the East coast of Africa to the eastern Pacific in a matter of days during the rapid decay of the El Niño and initiation of La Niña. Takayabu et al. (1999) suggest that an MJO influenced the termination of El Niño through the intensification of easterly trade winds.

A similar Hovmöller analysis was performed on the NCEP/NCAR data (not shown here). Globally, magnitudes of the modeled precipitation were smaller than those observed. The observations (Fig. 11) suggest that equatorial mesoscale complexes are an important mechanism for the transport of substantial rainfall amounts from the Maritime Continent to the East Pacific. However, in the reanalysis these systems are less well defined and there seems to be a large scale spreading of light precipitation across the basin. In fact, in early 1998 the model shows about equal precipitation amounts in the East and West Pacific. This helps explain why in the annual average the wettest area of the central Pacific is further West for NCEP/NCAR as compared to GPCPx (Fig. 10).

Finally, the NCEP/NCAR reanalysis produced continuous convective precipitation between 90° and 120° E during 1997-98, which is consistent with the small negative anomalies over the Maritime Continent in Fig. 10b.

Daily precipitation is useful for tracking the Madden-Julian 30-60 day oscillation and can even approximate the timing of westerly wind bursts in the Maritime Continent region. In a recent study, Yu and Rienecker (1998) documented a westerly wind burst event during the end of February and beginning of March 1997. At the same time there was a rapid eastward migration of convection off the Maritime Continent (Fig. 12). This phenomena was reflected in a precipitous drop in the mc- index (climatology was not subtracted out). In fact, from January to August 1997 the 30 day running mean of mc- is step-like, with the largest decrease during the February-March period. A lesser decrease occurred in July. The westerly wind burst event coincides with the beginning of an active Madden-Julian Oscillation (Fig. 11). Although the NCEP/NCAR model resolves the MJO, the rains over the Maritime Continent do not decrease over time. This may be a reason why the model does not show the large precipitation anomalies in the East Pacific in early 1998, and produces only a weak anomalous precipitation gradient in the Pacific basin during the ENSO.

6. Conclusions

This study examined global precipitation observations during the 1997-98 El Niño and beginning of the 1998-99 La Niña. Comparisons were made with NCEP/NCAR model output. Precipitation anomaly patterns during these years were in general consistent with the typical ENSO patterns described in previous studies, namely wet in the central to eastern Pacific, and southeastern U.S., and dry over the Maritime Continent and northeastern South America. The precipitation observations revealed strong precipitation anomalies over the Indian Ocean, southeast Pacific basin, North Atlantic, and other areas not well observed at the surface. The largest precipitation anomalies were confined to the equatorial Pacific basin and Maritime Continent from April to September 1997, were found throughout the global tropics and subtropics at the end of 1997, and extended as far poleward as Alaska by the beginning of 1998.

The evolution of the El Niño was tracked by a suite of SST and precipitation indices in the Pacific basin and Maritime Continent. Dry anomalies over the Maritime Continent and along the equator in the Pacific led the formation of the El Niño SST anomaly. It is conjectured that the anomalously clear conditions in the East Pacific contributed to warming at the surface through increased incoming solar radiation. In turn, the warming led to enhanced convection. Even while the El Niño strengthened, the seeds of the La Niña were observed as negative precipitation anomalies formed to the north of the equator. Much of the precipitation information was synthesized into the ENSO Precipitation Index (ESPI). The ESPI indicated that the zonal Walker circulation was weakest during boreal fall, before the SST anomalies in the eastern Pacific reached a maximum.

There were several discrepancies between the observed precipitation anomalies and those computed by the NCEP/NCAR model which were discovered by analyzing anomaly maps and time-longitude diagrams for the equatorial Pacific during 1997-98. The reanalysis product has a bias towards positive precipitation anomalies and the magnitudes of the anomalies in the equatorial Pacific are small as compared to the observations. The MJO was resolved by GPCPx and NCEP/NCAR, but the model did not show a substantial decrease in rainfall over the Maritime Continent which may have contributed to the weak positive precipitation anomalies in the East Pacific as compared to the observations.

Finally, one degree daily precipitation is not only useful for observing the MJO, but also for indicating the occurrence of westerly wind burst events. It has been shown that the wind bursts are associated with rapid movement of precipitation westward from the Maritime Continent to the West Pacific and that less precipitation returns after the event is over, thus leading to a step-down decrease of rainfall over the Maritime Continent. Two of these decreases occurred in late February and July 1997.

Future work will focus on using the 20 years of precipitation data to determine if the pattern of evolution of the 1997-98 El Niño and 1998-99 La Niña can be observed in other ENSO events. This information would be beneficial to climate prediction.

Acknowledgements: This research is supported through the TRMM Science Team and NASA's Atmospheric Dynamics and Thermodynamics Program under Dr. Ramesh Kakar

Figure Captions

Fig. 1. Global precipitation anomalies from the long-term 1987-98 mean averaged for the year April 1997 to March 1998. Shading and thin dashed contours denote negative values and solid contours positive values. (a) Precipitation anomaly contour intervals are 2 mm day^{-1} . Thick lines contain areas with consistent El Niño precipitation signal from Ropelewski and Halpert (1987, Fig. 21). Solid-lined areas are wet and dashed-lined areas are dry. (b) Anomalies divided by the standard deviations. Contour intervals are unity and begin at ± 2 .

Fig. 2. Orientation map. The large solid-lined and dashed-lined boxes indicate the Pacific (p) and Maritime Continent (mc) regions respectively. Shaded regions mark the locations of INDO (5N, 5S; 90E, 140E) and NINO 3.4 (5N, 5S; 170W, 120W) and represent the areas over which A_{mc} and A_p are computed.

Fig. 3. Bimonthly averages of SST (a, c, e, g) and precipitation anomalies (b, d, f, h) from January to August 1997. Thin dashed contours and shading indicate negative values. Contours are in $2 \text{ }^\circ\text{C}$ increments for SST ranging from -5 to $5 \text{ }^\circ\text{C}$ and 4 mm day^{-1} increments for precipitation ranging from -10 to 10 mm day^{-1} . (a) SST January-February (Jan-Feb), (b) Precipitation Jan-Feb, (c) SST March-April (Mar-Apr), (d) Precipitation Mar-Apr, (e) SST May-June (May-Jun), (f) Precipitation May-Jun, (g) SST July-August (Jul-Aug), (h) Precipitation Jul-Aug.

Fig. 4. Same as Fig. 3; period from September 1997 to April 1998. (a) SST September-October (Sep-Oct), (b) Precipitation Sep-Oct, (c) SST November-December (Nov-Dec), (d) Precipitation Nov-Dec, (e) SST January-February 1998 (Jan-Feb), (f) Precipitation Jan-Feb, (g) SST March-April (Mar-Apr), (h) Precipitation Mar-Apr.

Fig. 5. Same as Fig. 3; period from May to December 1998. (a) SST May-June (May-Jun), (b) Precipitation May-Jun, (c) SST July-August (Jul-Aug), (d) Precipitation Jul-Aug, (e) SST September-October (Sep-Oct), (f) Precipitation Sep-Oct, (g) SST November-December (Nov-Dec), (h) Precipitation Nov-Dec.

Fig. 6. Same as Fig. 3; period from January to April 1999. (a) SST January-February (Jan-Feb), (b) Precipitation Jan-Feb, (c) SST March-April (Mar-Apr), (d) Precipitation Mar-Apr.

Fig. 7. 1996-98 time series of monthly sea surface temperature (SST) and bi-monthly precipitation indices for the central Pacific and Maritime Continent (ref. Fig. 2). For panels (a)-(c) thick lines connect the zero points to the maximum anomalies during the 97-98 El Niño. For panel (d) thick lines connect the zero points to the ends of the plots. (a) Solid line tracks Nino 3.4 (5N-5S, 170W-120W) and dashed line the INDO SST index (5N-5S, 90E-140E). (b) Solid and dashed lines track observed precipitation anomalies averaged over the Nino 3.4 and INDO areas respectively. (c) Solid and dashed lines denote observed Ap+ and Amc- precipitation indices respectively. (d) Solid and dashed lines denote observed Amc+ and Ap- precipitation indices respectively.

Fig. 8. 1996-98 time series of bi-monthly indices of anomalous precipitation gradient in the equatorial Pacific. Solid line tracks the ENSO Precipitation Index (ESPI), short-dashed line El Niño Index (EI), and long-dashed line La Niña Index (LI). Thick lines connect the zero points to the maximum anomalies during the 97-98 El Niño.

Fig. 9. 1996-98 time series of indices described in Fig. 7 derived from both observation (thin lines) and model (thick lines). (a) Solid and dashed lines track precipitation anomalies averaged over the Niño 3.4 and INDO areas respectively. (b) Solid and dashed lines denote Ap+ and Amc- precipitation indices respectively. (c) Solid and dashed lines denote Amc+ and Ap- precipitation indices respectively.

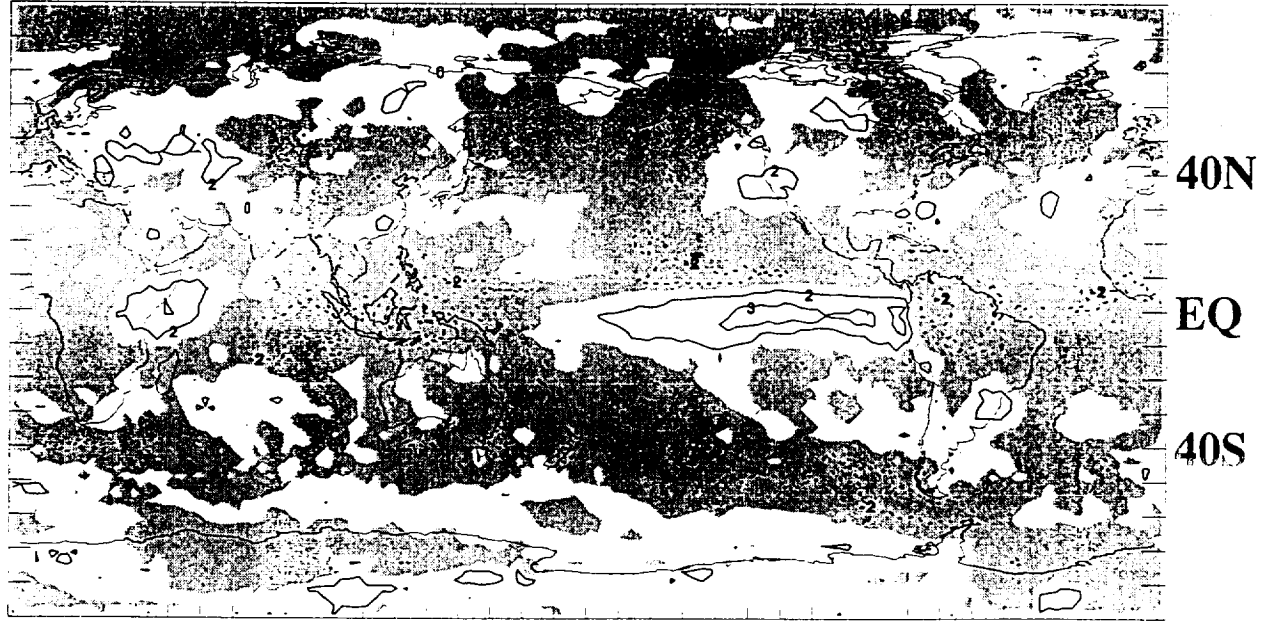
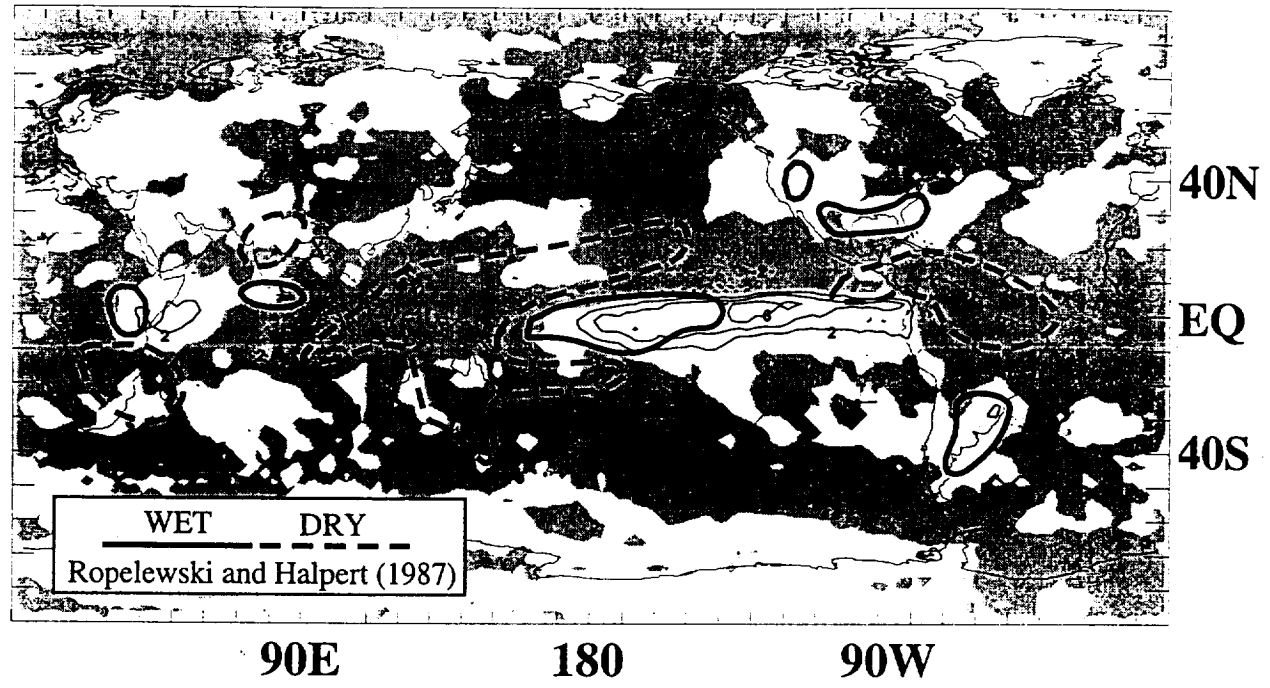
Fig. 10. Precipitation anomalies averaged for the year April 1997 to March 1998. Base period is 1987-96. Shading denotes positive values. Spacing is 2 mm day⁻¹.

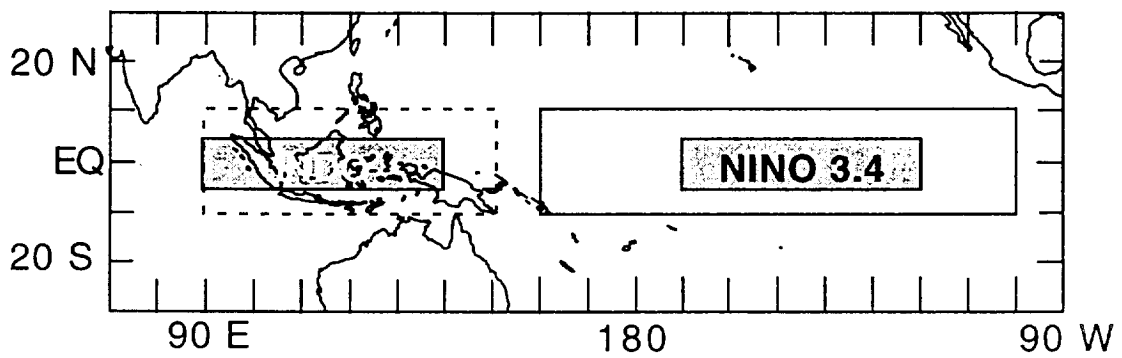
(a) GPCPx, (b) NCEP/NCAR, (c) the difference GPCPx minus NCEP/NCAR.

Fig. 11. Time-longitude diagram (5° N to 5° S) of global precipitation derived from an experimental one degree daily product. Period is January 1 1997 to December 31 1998. Color bar denotes precipitation rates from 0 to 20 mm day⁻¹.

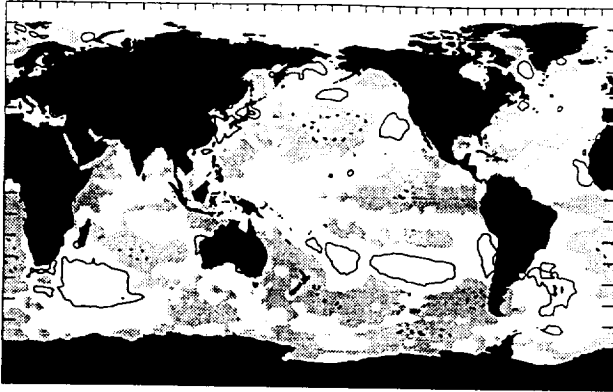
Fig. 12. Experimental one degree daily precipitation during a westerly wind burst event in late February 1997. mc- is plotted in mm day⁻¹ for 1997 and during the period February 10 to March 10. Thick line in top panel is 30-day running mean. Precipitation fields are shown for February 22, February 26, and March 4, where shading is delineated every 5 mm day⁻¹. Black denotes rain rates in excess of 5 mm day⁻¹, white rain rates in excess of 25 mm day⁻¹.

Global Precipitation Anomalies, Apr 97 to Mar 98

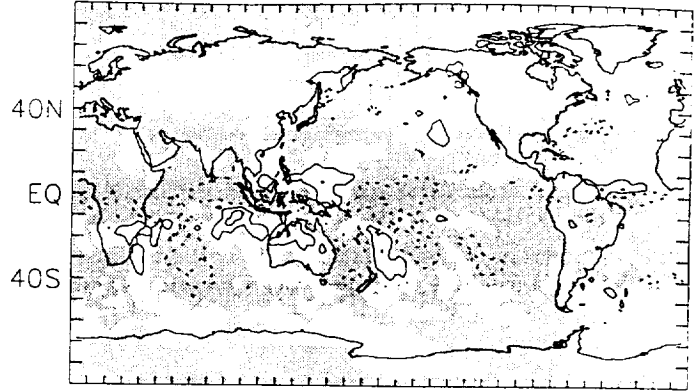




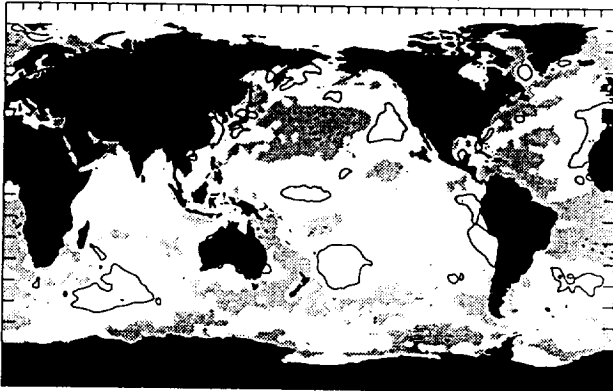
SST Anomalies Jan-Feb 97



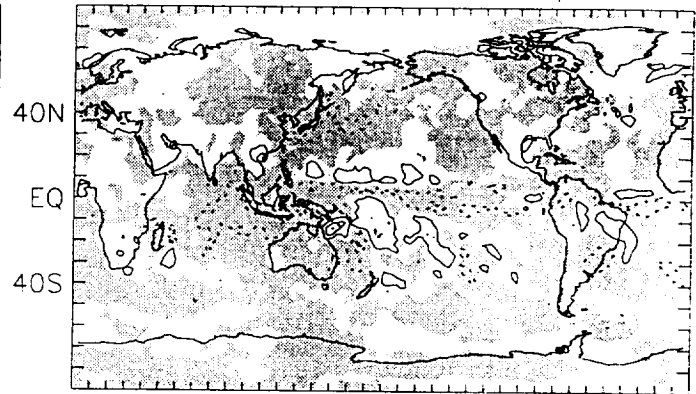
Precip. Anomalies Jan-Feb 97



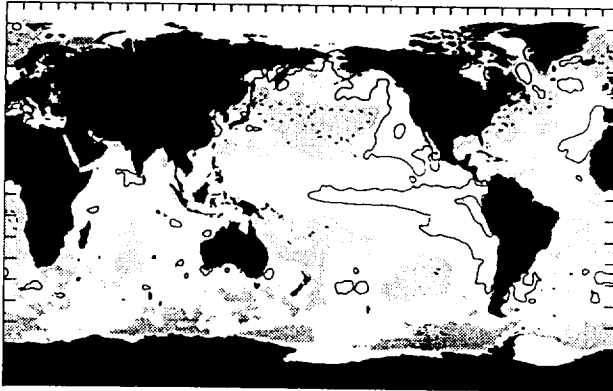
SST Anomalies Mar-Apr 97



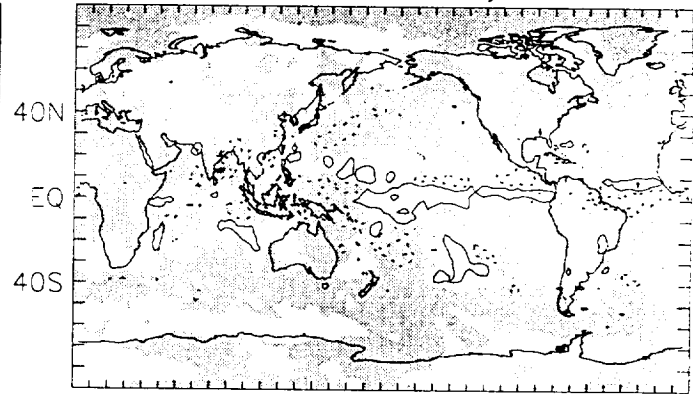
Precip. Anomalies Mar-Apr 97



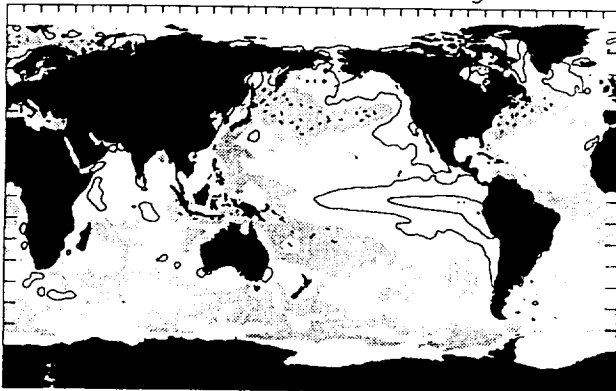
SST Anomalies May-Jun 97



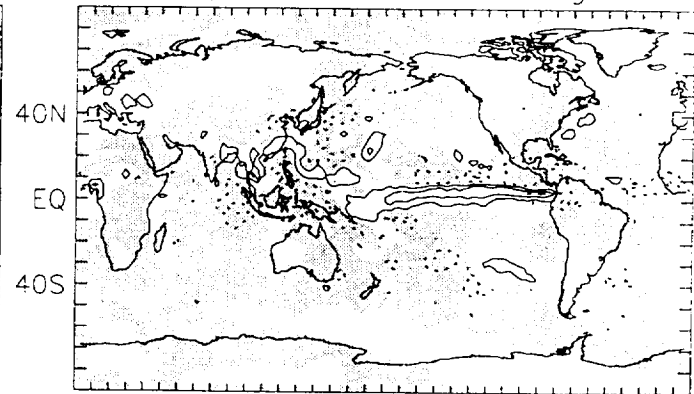
Precip. Anomalies May-Jun 97



SST Anomalies Jul-Aug 97



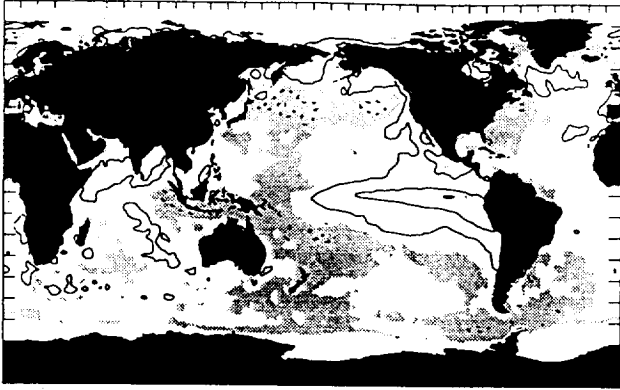
Precip. Anomalies Jul-Aug 97



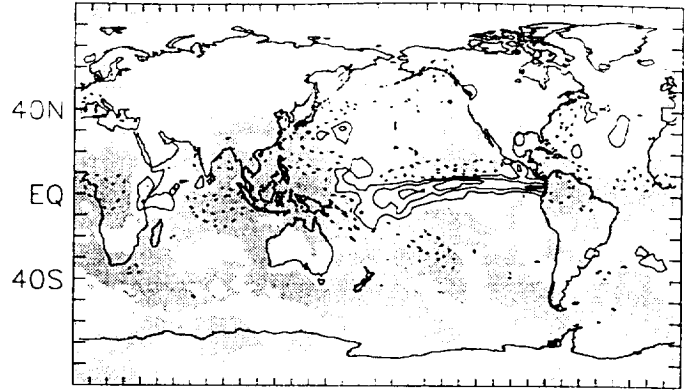
90E 180 90W

90E 180 90W

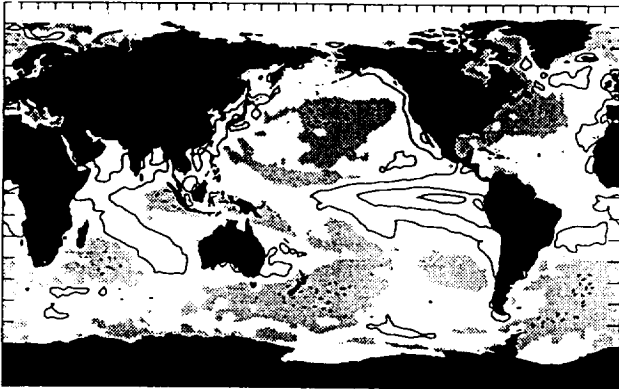
SST Anomalies Sep-Oct 97



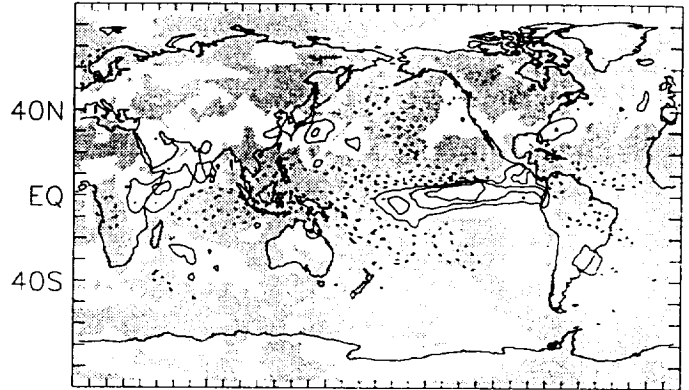
Precip. Anomalies Sep-Oct 97



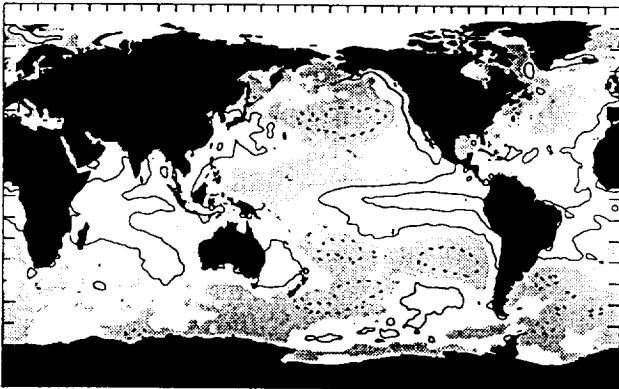
SST Anomalies Nov-Dec 97



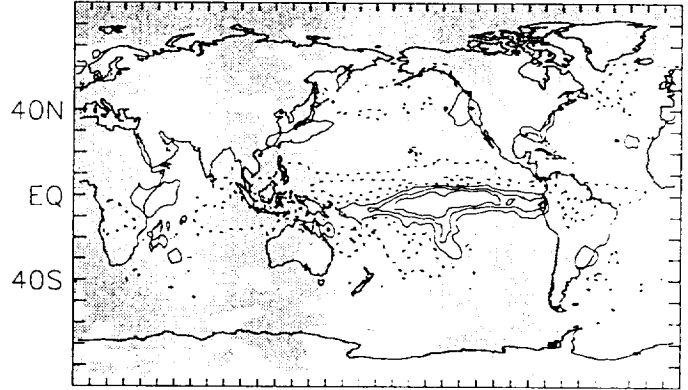
Precip. Anomalies Nov-Dec 97



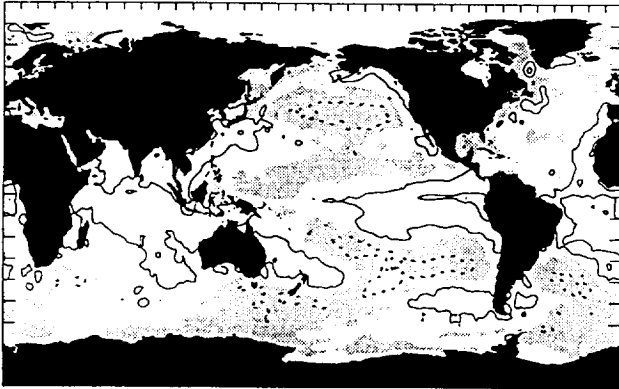
SST Anomalies Jan-Feb 98



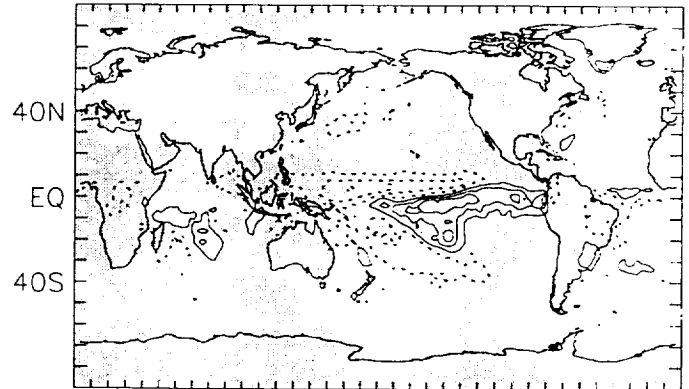
Precip. Anomalies Jan-Feb 98



SST Anomalies Mar-Apr 98



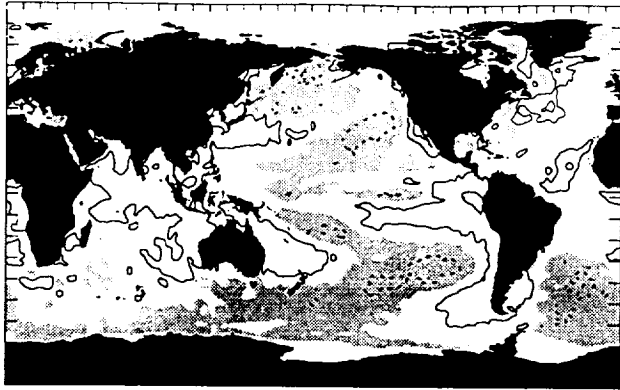
Precip. Anomalies Mar-Apr 98



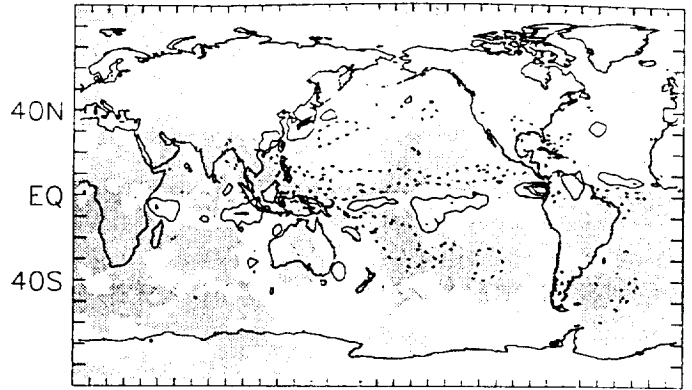
90E 180 90W

90E 180 90W

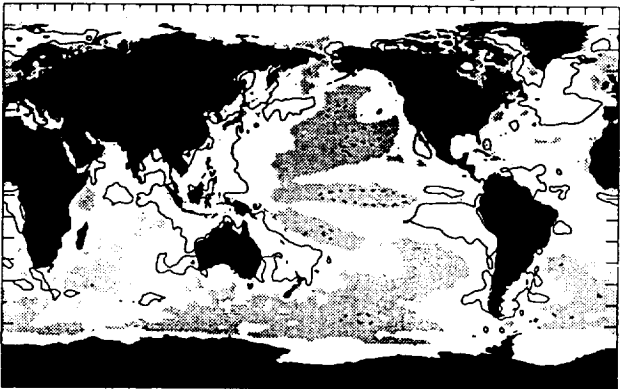
SST Anomalies May-Jun 98



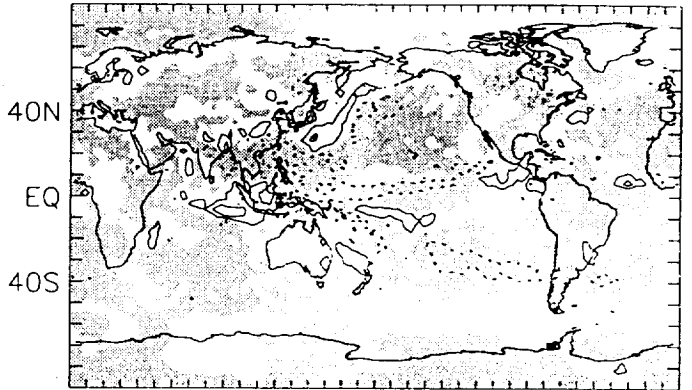
Precip. Anomalies May-Jun 98



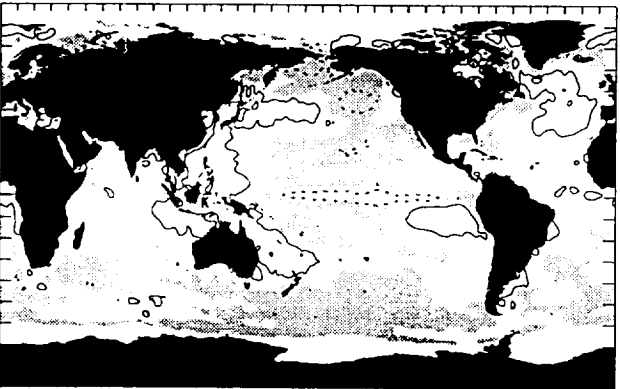
SST Anomalies Jul-Aug 98



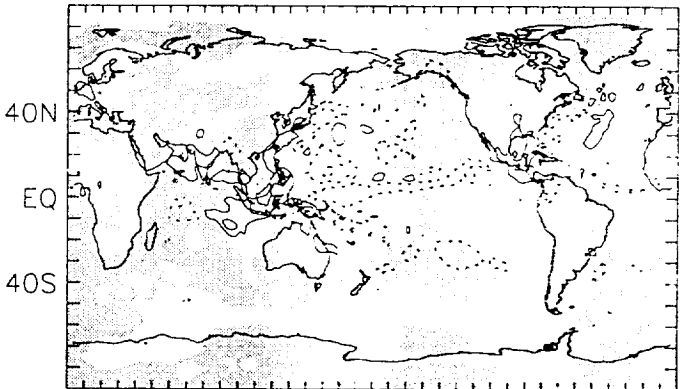
Precip. Anomalies Jul-Aug 98



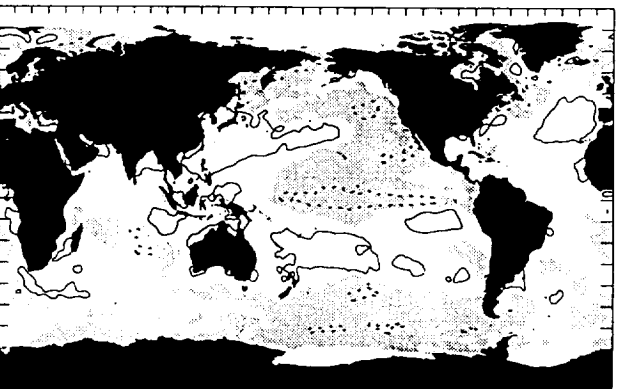
SST Anomalies Sep-Oct 98



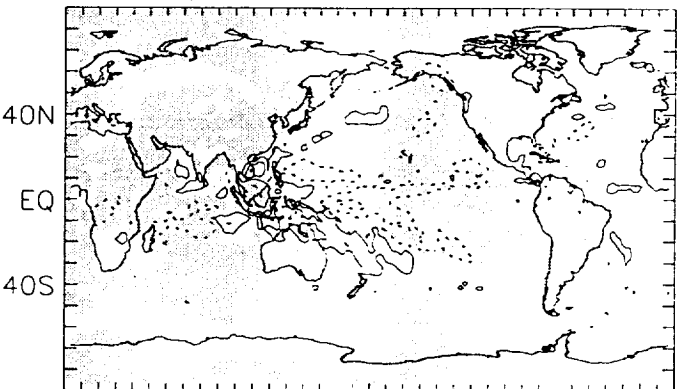
Precip. Anomalies Sep-Oct 98



SST Anomalies Nov-Dec 98



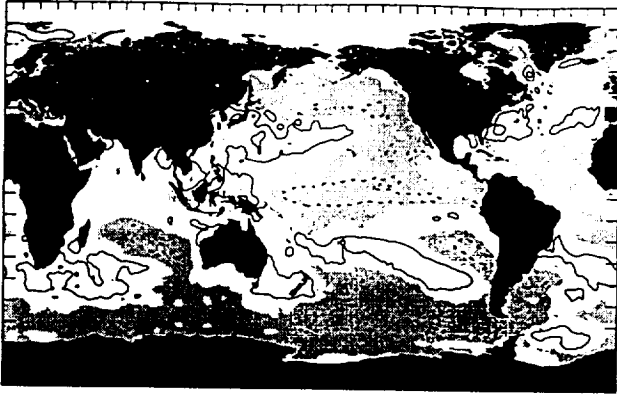
Precip. Anomalies Nov-Dec 98



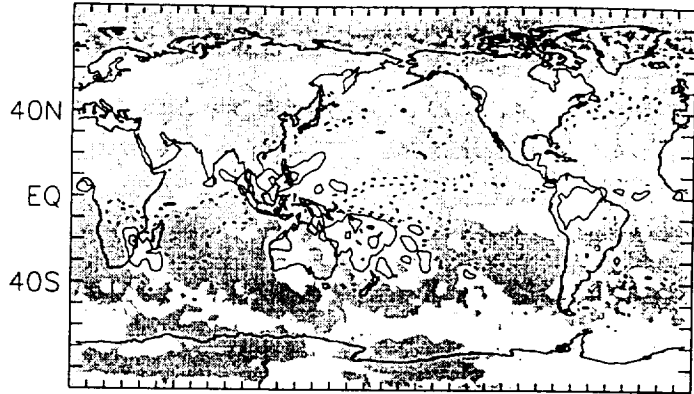
90E 180 90W

90E 180 90W

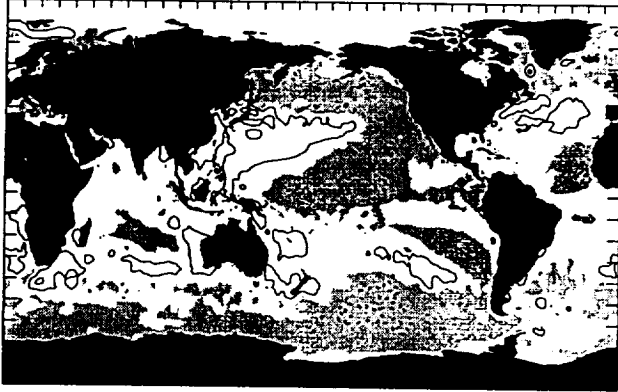
SST Anomalies Jan-Feb 99



Precip. Anomalies Jan-Feb 99

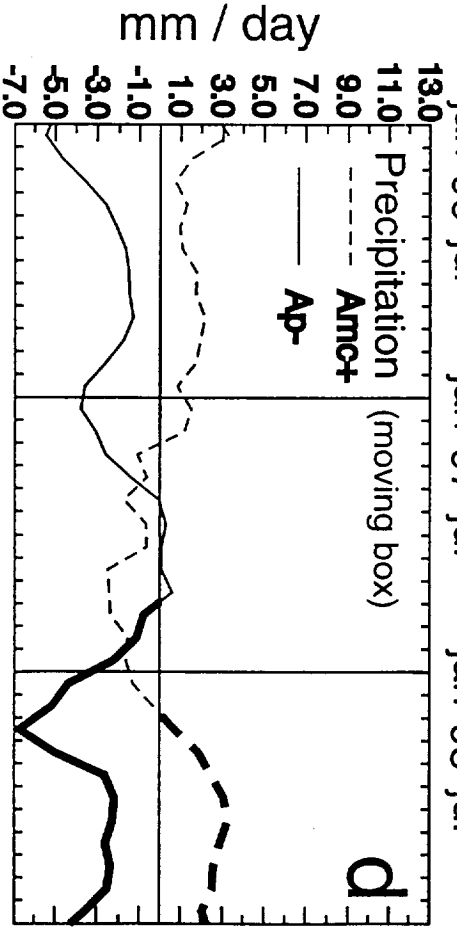
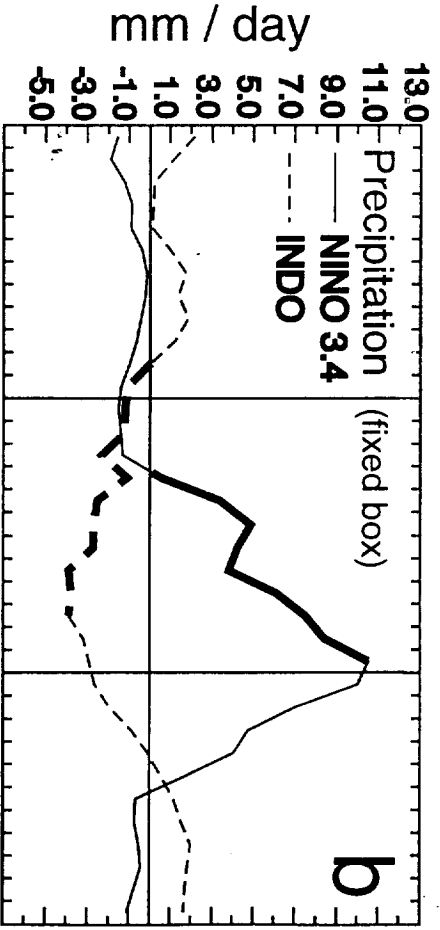
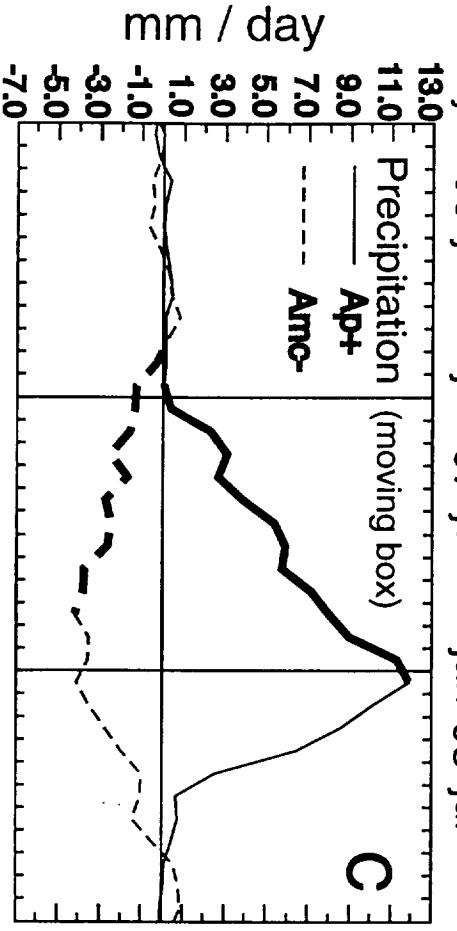
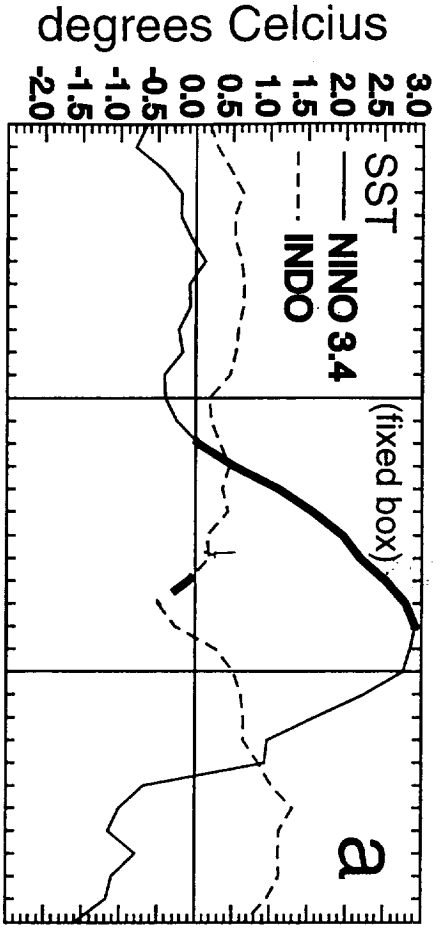


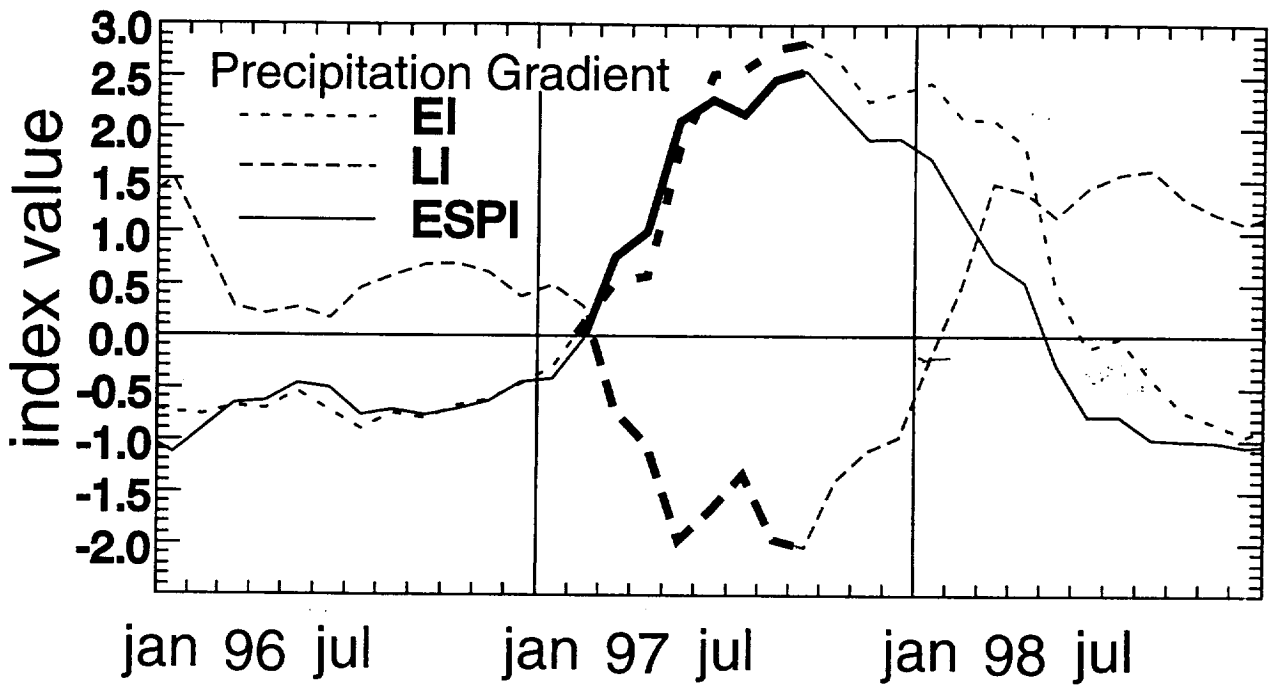
SST Anomalies Mar-Apr 99

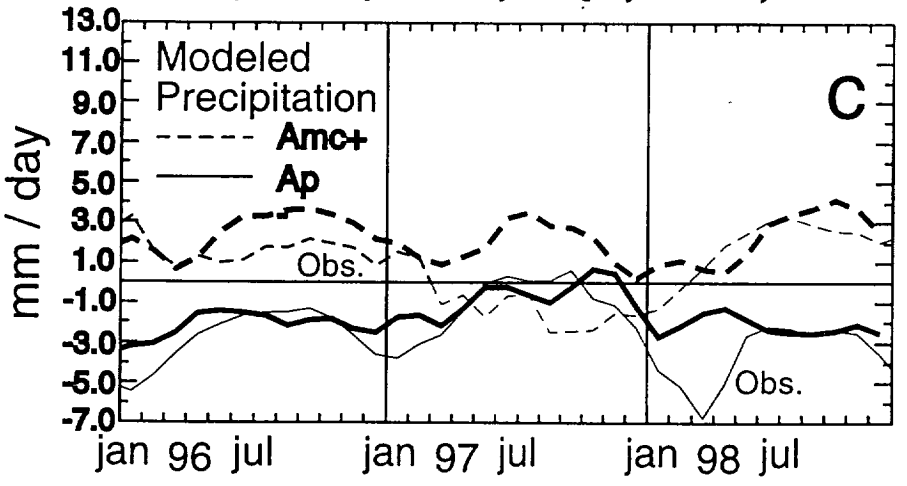
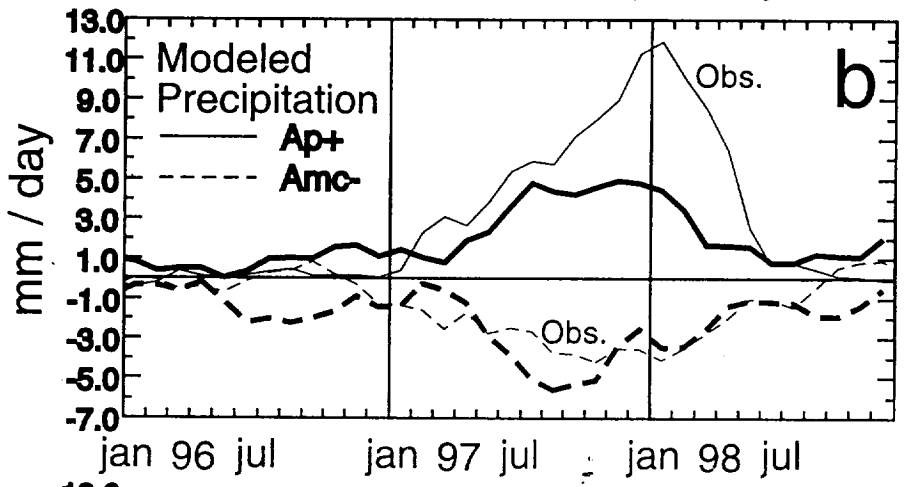
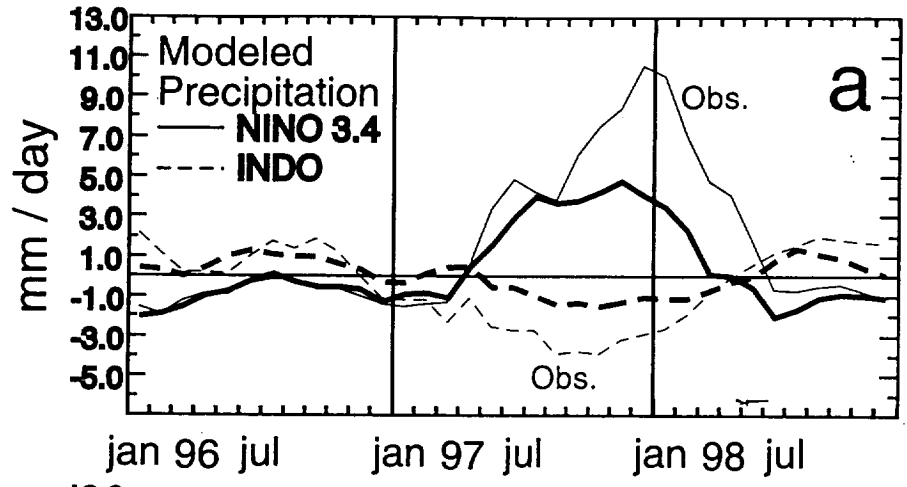


Precip. Anomalies Mar-Apr 99

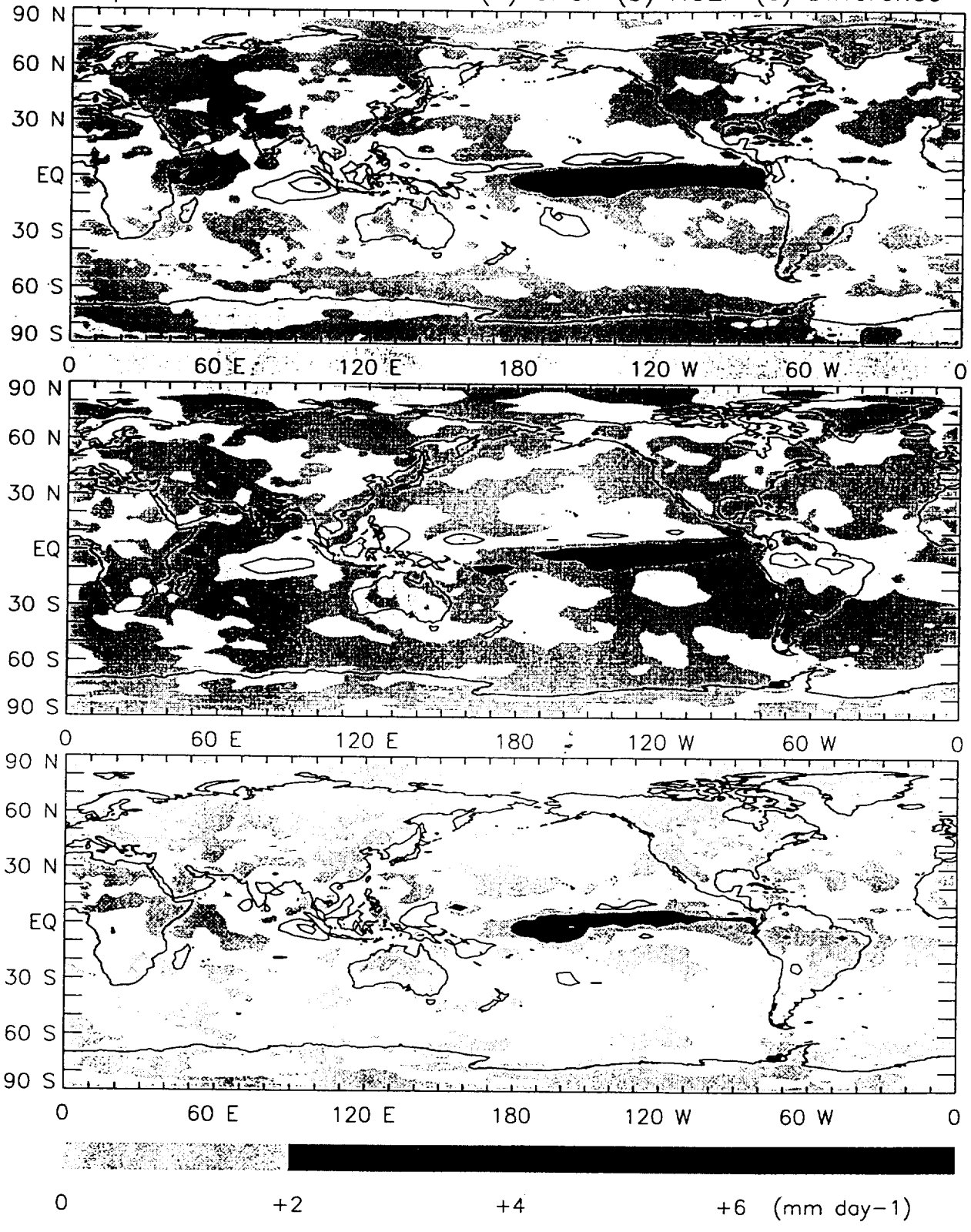






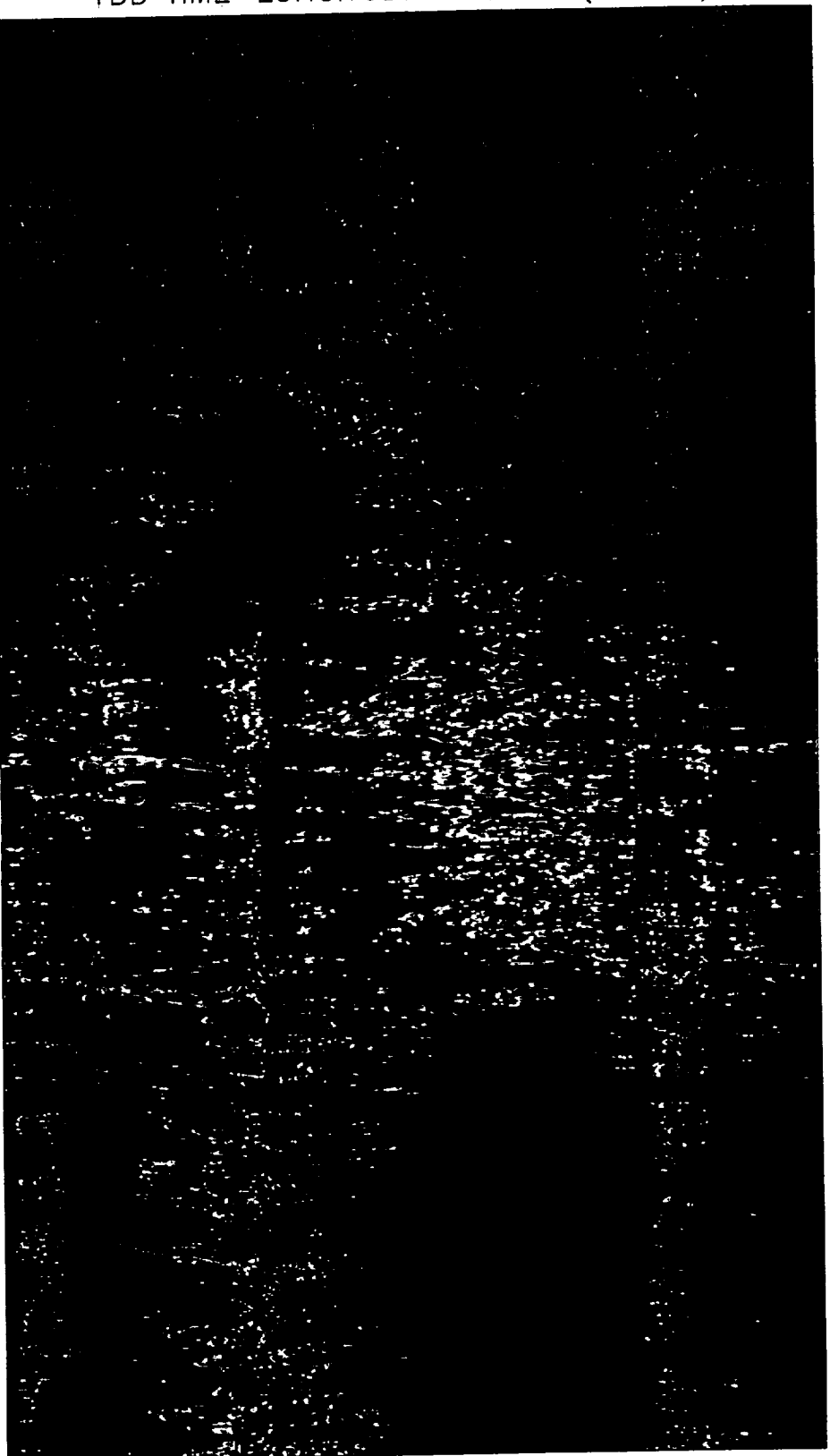


April 1997 to March 1998 (a) GPCP (b) NCEP (c) Difference

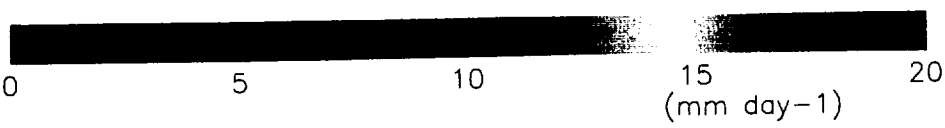


1DD TIME-LONGITUDE DIAGRAM (5N-5S)

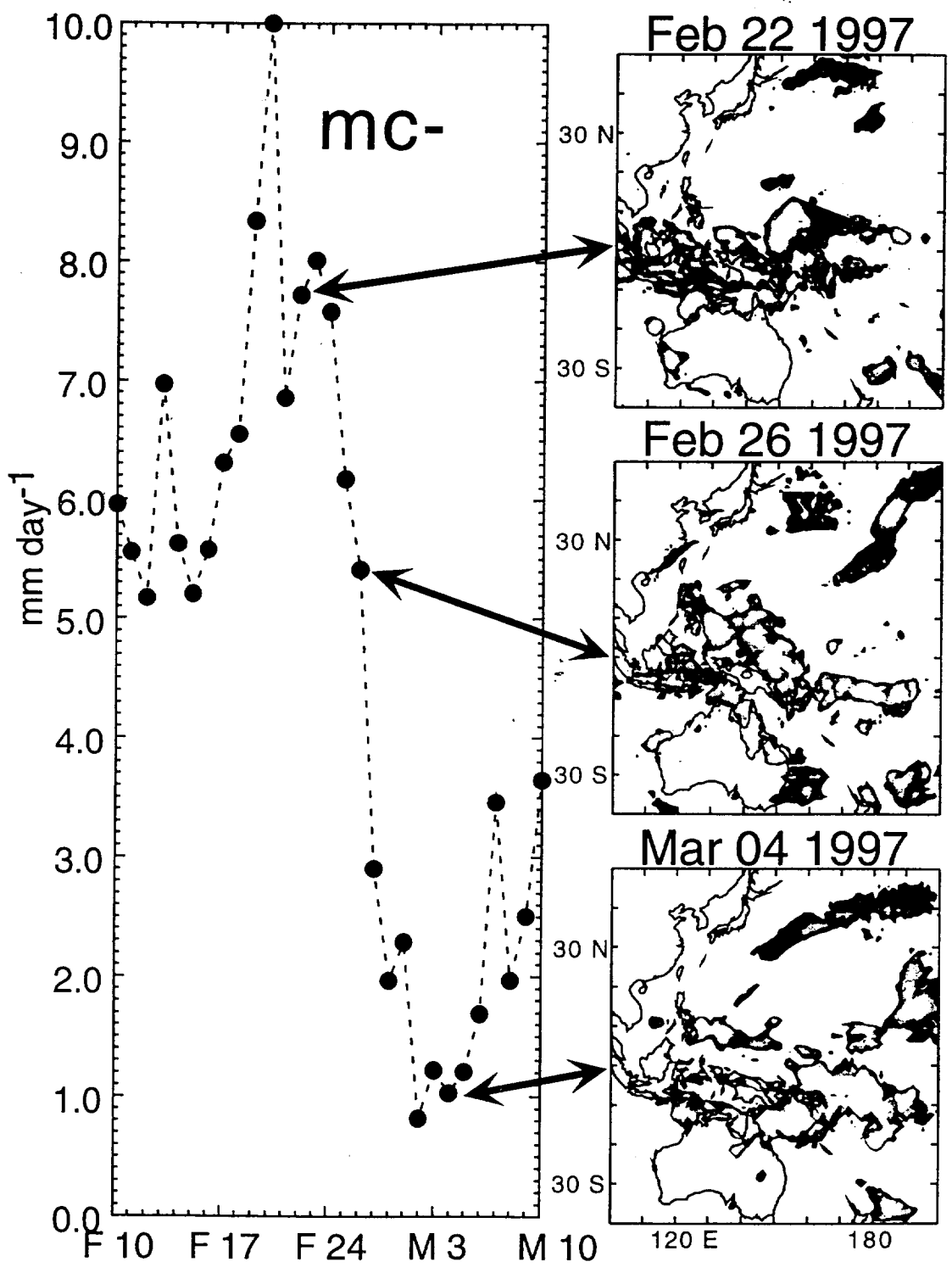
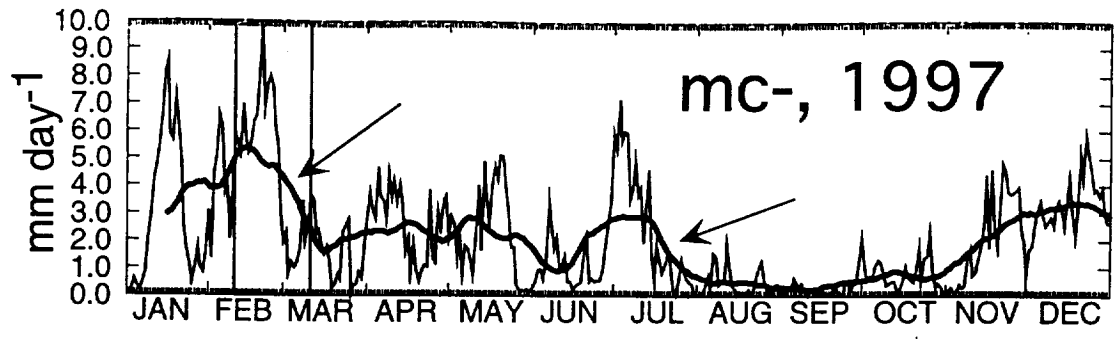
JAN 1
97
FEB 1
MAR 1
APR 1
MAY 1
JUN 1
JUL 1
AUG 1
SEP 1
OCT 1
NOV 1
DEC 1
JAN 1
98
FEB 1
MAR 1
APR 1
MAY 1
JUN 1
JUL 1
AUG 1
SEP 1
OCT 1
NOV 1
DEC 1



0 40 E 80 120 160 E 160 W 120 80 40 W 0



15
(mm day-1)



References:

Bell, G. D. and M. S. Halpert, 1998: Climate assessment for 1997. *Bull. Amer. Meteor. Soc.*, **79**, S1-S50.

Bell, G. D., M. S. Halpert, C. F. Ropelewski, V. E. Kousky, A. V. Douglas, R. C. Schnell, and M. E. Gelman, 1999: Climate assessment for 1998. *Bull. Amer. Meteor. Soc.*, **80**, S1-S48.

Curtis, S. and R. Adler, 1999: Precipitation-based ENSO indices. *J. Climate*, submitted.

Curtis, S. and S. Hastenrath, 1997: Interannual variability of circulation and climate in the tropical Pacific and Australasia related to the Southern Oscillation. *J. Meteor. Soc. Japan*, **75**, 819-829.

Harrison, D. E. and N. K. Larkin, 1998: Seasonal U.S. temperature and precipitation anomalies associated with El Niño: Historical results and comparison with 1997-98. *Geophys. Res. Lett.*, **25**, 3959-3962.

Huffman, G. J., R. F. Adler, P. Arkin, A. Chang, R. Ferraro, A. Gruber, J. Janowiak, A. McNab, B. Rudolf, U. Schneider, 1997: The Global Precipitation Climatology Project (GPCP) combined precipitation dataset. *Bull. Amer. Meteor. Soc.*, **78**, 5-20.

Huffman, G. J., R. F. Adler, and D. Bolvin, 1999: Description and Examples of Daily 1x1-Degree Precipitation Estimates. *Proceedings from the 3rd International Scientific Conference on the Global Energy and Water Cycle*, Beijing, China, June 1999.

Jaksic, F. M., 1998: The multiple facets of El Niño Southern Oscillation in Chile. *Revista Chilena de Historia Natural*, 71, 121-131.

Janowiak, J., A. Gruber, C. R. Kondragunta, R. E. Livezey, and G. J. Huffman, 1998: A comparison of the NCEP-NCAR reanalysis precipitation and the GPCP rain gauge-satellite combined dataset with observational error considerations. *J. Climate*, 11, 2960-2979.

Jensen, M. P., J. H. Mather, and T. P. Ackerman, 1998: Observations of the 1997-98 warm ENSO event at the Manus Island ARM site. *Geophys. Res. Lett.*, 25, 4517-4520.

Kalnay, E., M. Kanamitsu, R. Kistler, W. Collins, D. Deaven, L. Gandin, M. Iredell, S. Saha, G. White, J. Woollen, Y. Zhu, M. Chelliah, W. Ebisuzaki, W. Higgins, J. Janowiak, K. C. Mo, C. Ropelewski, J. Wang, A. Leetmaa, R. Reynolds, R. Jenne, and D. Joseph, 1996: The NCEP/NCAR 40-year reanalysis project. *Bull. Amer. Meteor. Soc.*, 77, 437-471.

Kogan, F. N., 1998: A typical pattern of vegetation conditions in southern Africa during El Niño years detected from AVHRR data using three-channel numerical index. *Int. J. of Remote Sensing*, 19, 3689-3695.

Mc Phadden, M. J., 1999: Climate oscillations - Genesis and evolution of the 1997-98 El Niño. *Science*, 283, 950-954.

Montroy, D. L., M. B. Richman, and P. J. Lamb, 1998: Observed nonlinearities of monthly teleconnections between tropical Pacific sea surface temperature anomalies and central and eastern North American precipitation. *J. Climate*, 11, 1812-1835.

Mullen, C., 1998: Seasonal climate summary southern hemisphere (summer 1997/98): warm event (El Niño) continues. *Australian Meteorological Magazine*, 47, 253-259.

Pavia, E. G. and A. Badan, 1998: ENSO modulates rainfall in the Mediterranean Californias, *Geophys. Res. Lett.*, 25, 3855-3858.

Reynolds, R. W. and T. M. Smith, 1995: A high-resolution global sea surface temperature climatology, *J. Climate*, 8, 1571-1583.

- Ropelewski, C. F. and M. S. Halpert, 1987: Global and regional scale precipitation patterns associated with the El Niño/Southern Oscillation. *Mon. Wea. Rev.*, 115, 1606-1626.
- Susskind, J., P. Piraino, L. Rokke, L. Iredell, and A. Mehta, 1997: Characteristics of the TOVS pathfinder path A dataset. *Bull. Amer. Meteor. Soc.*, 78, 1449-1472.
- Takayabu, Y. N., T. Iguchi, M. Kachi, A. Shibata, and H. Kanzawa, 1999: An impact of the Madden-Julian oscillation on the abrupt termination of the 1997-98 El Niño, *Nature*, submitted.
- Yu, L. and M. R. Rienecker, 1998: Evidence of an extratropical atmospheric influence during the onset of the 1997-98 El Niño. *Geophys. Res. Lett.*, 25, 3537-3540.